NASA/TM-2005-212861

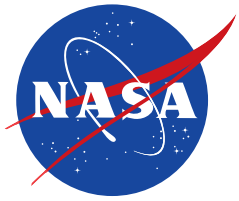

Twist Model Development and Results From the Active Aeroelastic Wing F/A-18 Aircraft

Andrew M. Lizotte and Michael J. Allen
NASA Dryden Flight Research Center
Edwards, California

March 2005

The NASA STI Program Office…in Profile

Since its founding, NASA has been dedicated to the advancement of aeronautics and space science. The NASA Scientific and Technical Information (STI) Program Office plays a key part in helping NASA maintain this important role.

The NASA STI Program Office is operated by Langley Research Center, the lead center for NASA's scientific and technical information. The NASA STI Program Office provides access to the NASA STI Database, the largest collection of aeronautical and space science STI in the world. The Program Office is also NASA's institutional mechanism for disseminating the results of its research and development activities. These results are published by NASA in the NASA STI Report Series, which includes the following report types:

- TECHNICAL PUBLICATION. Reports of completed research or a major significant phase of research that present the results of NASA programs and include extensive data or theoretical analysis. Includes compilations of significant scientific and technical data and information deemed to be of continuing reference value. NASA's counterpart of peer-reviewed formal professional papers but has less stringent limitations on manuscript length and extent of graphic presentations.

- TECHNICAL MEMORANDUM. Scientific and technical findings that are preliminary or of specialized interest, e.g., quick release reports, working papers, and bibliographies that contain minimal annotation. Does not contain extensive analysis.

- CONTRACTOR REPORT. Scientific and technical findings by NASA-sponsored contractors and grantees.

- CONFERENCE PUBLICATION. Collected papers from scientific and technical conferences, symposia, seminars, or other meetings sponsored or cosponsored by NASA.

- SPECIAL PUBLICATION. Scientific, technical, or historical information from NASA programs, projects, and missions, often concerned with subjects having substantial public interest.

- TECHNICAL TRANSLATION. English-language translations of foreign scientific and technical material pertinent to NASA's mission.

Specialized services that complement the STI Program Office's diverse offerings include creating custom thesauri, building customized databases, organizing and publishing research results…even providing videos.

For more information about the NASA STI Program Office, see the following:

- Access the NASA STI Program Home Page at ***http://www.sti.nasa.gov***

- E-mail your question via the Internet to help@sti.nasa.gov

- Fax your question to the NASA STI Help Desk at (301) 621-0134

- Telephone the NASA STI Help Desk at (301) 621-0390

- Write to:
  NASA STI Help Desk
  NASA Center for AeroSpace Information
  7121 Standard Drive
  Hanover, MD 21076-1320

NASA/TM-2005-212861

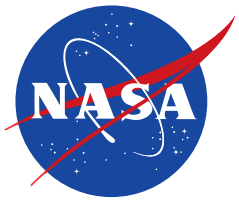

Twist Model Development and Results From the Active Aeroelastic Wing F/A-18 Aircraft

Andrew M. Lizotte and Michael J. Allen
NASA Dryden Flight Research Center
Edwards, California

National Aeronautics and
Space Administration

Dryden Flight Research Center
Edwards, California 93523-0273

March 2005

NOTICE

Use of trade names or names of manufacturers in this document does not constitute an official endorsement of such products or manufacturers, either expressed or implied, by the National Aeronautics and Space Administration.

Available from the following:

NASA Center for AeroSpace Information (CASI)
7121 Standard Drive
Hanover, MD 21076-1320
(301) 621-0390

National Technical Information Service (NTIS)
5285 Port Royal Road
Springfield, VA 22161-2171
(703) 605-6000

ABSTRACT

Understanding the wing twist of the active aeroelastic wing F/A-18 aircraft is a fundamental research objective for the program and offers numerous benefits. In order to clearly understand the wing flexibility characteristics, a model was created to predict real-time wing twist. A reliable twist model allows the prediction of twist for flight simulation, provides insight into aircraft performance uncertainties, and assists with computational fluid dynamic and aeroelastic issues.

The left wing of the aircraft was heavily instrumented during the first phase of the active aeroelastic wing program allowing deflection data collection. Traditional data processing steps were taken to reduce flight data, and twist predictions were made using linear regression techniques. The model predictions determined a consistent linear relationship between the measured twist and aircraft parameters, such as surface positions and aircraft state variables. Error in the original model was reduced in some cases by using a dynamic pressure-based assumption and by using neural networks. These techniques produced excellent predictions for flight between the standard test points and accounted for nonlinearities in the data. This report discusses data processing techniques and twist prediction validation, and provides illustrative and quantitative results.

NOMENCLATURE

AAW	active aeroelastic wing
C_i	equation coefficient for the i^{th} parameter input
C_t	DPA equation intercept coefficient
DPA	dynamic pressure assumption
EQDE	EQuation DErivation
FDMS	flight deflection measurement system
i	parameter input number
I	intercept
I_i	DPA intercept for the i^{th} parameter input
ILEF	inboard leading-edge flap
I_t	DPA intercept coefficient
k	number of samples
l	sample number
LAilLVDT	left aileron linear variable displacement transducer
LED	light emitting diode
LOLEFRVDT	left outboard leading-edge flap rotary variable displacement transducer

M_l	measured twist of sample number l
n	number of parameter inputs
OBES	onboard excitation system
OLEF	outboard leading-edge flap
PCM	pulse code modulation
P_i	i^{th} model parameter input
$\bar{q}$	dynamic pressure
R_l	predicted twist of sample l
RMS	root mean square
RMS_{Norm}	normalized root mean square
TEF	trailing-edge flap
T_{Range}	twist angle range
Δ	vertical displacement difference
δ	fixed distance (chordwise spacing) between two target locations
θ	angle of twist

INTRODUCTION

This study investigates the process to determine and evaluate elastic streamwise twist predictions on the left wing of the active aeroelastic wing (AAW) aircraft. Understanding the wing twist onboard the AAW is a fundamental research objective for the program and offers numerous benefits. A reliable model allows the ability to predict twist in flight simulation, provides knowledge into aircraft performance uncertainties, and assists with computational fluid dynamic and aeroelastic issues.

The electro-optical flight deflection measurement system (FDMS)[1] was used to record absolute displacement at 16 different locations on the AAW left wing during phase-1 of the flight program. Resultant wing-twist time histories were calculated at four of the six available stations across the wingspan using the collected deflection data. The model objective was to predict measured twist using a multiple linear regression technique based on aircraft state variable and surface position characteristics. The following sections detail the process of creating a model to predict twist and determine technique reliability in twist predictions. Documentation includes the instrumentation setup, data acquisition and processing, and linear regression method used to develop the twist model. Other methods, such as a dynamic pressure-based assumption and a neural net technique, were also used to further reduce error in original model twist predictions. Illustrative and quantitative results are presented for the model as well as analysis of anomalies and nonintuitive results.

BACKGROUND AND DATA PROCESSING

Analysis referred to in this report was performed with twist data measured on the AAW aircraft, a modified F/A-18 fighter as shown in figure 1. Changes on the aircraft to incorporate AAW technology include two major modifications.[2] Thinner panels replaced most top and bottom aft wing box panels, thereby increasing wing flexibility. This structural change made the AAW wing flexibility similar to that of original preproduction wings. Secondly, the inboard leading-edge flap (ILEF) and outboard leading-edge flap (OLEF) were decoupled to allow independent control of each surface. Typically, ILEFs and OLEFs are physically connected and must be controlled together. Separate controls and drives were implemented to control each leading-edge surface and allowed increased surface travel. These changes were the first stage in an effort to achieve the AAW program main objective to demonstrate roll control using wing twist. By integrating aerodynamics, flight controls, and structures, aeroelastic deformation of the wing may be used for a net benefit in roll control. Future aircraft designs using AAW research could enable higher aspect ratio and thinner and more flexible wings, which provide improved fuel efficiency from reduced aircraft weight and decreased aerodynamic drag. The AAW program is a joint effort between the Air Force Research Laboratory (AFRL), Boeing's Phantom Works (St. Louis, Missouri), and NASA Dryden Flight Research Center (DFRC, Edwards, California).

EC03-0039-14

Figure 1. AAW aircraft, modified F/A-18 fighter, 360-deg roll.

Instrumentation Description

Vertical structural deflections of the AAW left wing were measured in flight using the FDMS. Figure 2(a) shows the sixteen infrared light emitting diodes (LEDs) that were installed on the upper surface of the wing where the aeroelastically deformed surface could be measured. The targets were scanned sequentially beginning with target 0 and ending with target 15. Sequencing through the 16 LED targets took 80 ms, at which time the sequence began again with target 0, thus producing a sampling rate of 12.5 samples/s for each target. This sampling rate was adequate for quasi-static structural measurements, even for high-rate maneuvers such as abrupt step commands to the control surfaces.[3]

Light from the target LED was focused as a line on a light-sensitive diode array mounted at the lens focal point. The receiver relayed to the control unit an electrical signal proportional to the point at which the target light encounters the diode array. Figure 2(b) shows an outboard view of the two optical receivers, which were mounted in the pod just aft of the cockpit to receive target data. A 10-cm focal length receiver was used to view inboard targets 0 through 9, while a 20-cm focal length receiver viewed the outboard targets 10 through 15. Combining two receivers allowed complete field-of-view coverage and optimized resolution. The control unit, which contains the logic necessary to operate the FDMS, also served to interface the FDMS with the pulse code modulation (PCM) data-recording system. The deflection data were recorded as two 10-bit digital words. One word contained position data and the other contained the target identification and error messages. After acquired by the PCM system, the data were transmitted to a ground station for recording. Previous applications of the FDMS technology include the highly maneuverable aircraft technology (HiMAT),[4] X-29 forward-swept wing aircraft,[3] advanced fighter technology integration (AFTI) F-111 mission adaptive wing research aircraft,[5,6] and F-16C Block 40 aircraft.[7]

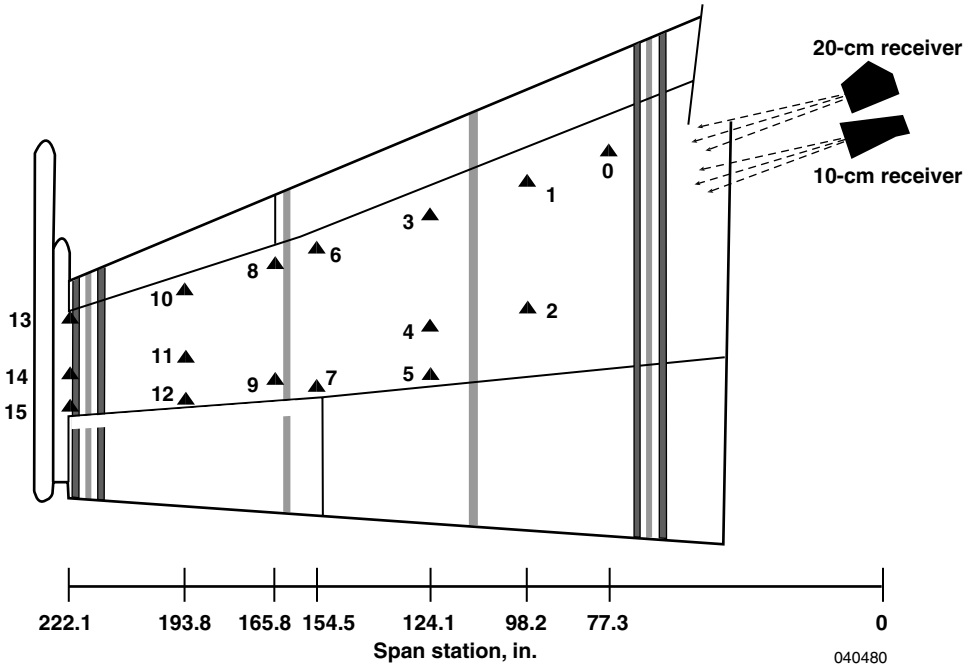

(a) Top view sketch with span station.

Figure 2. FDMS setup.

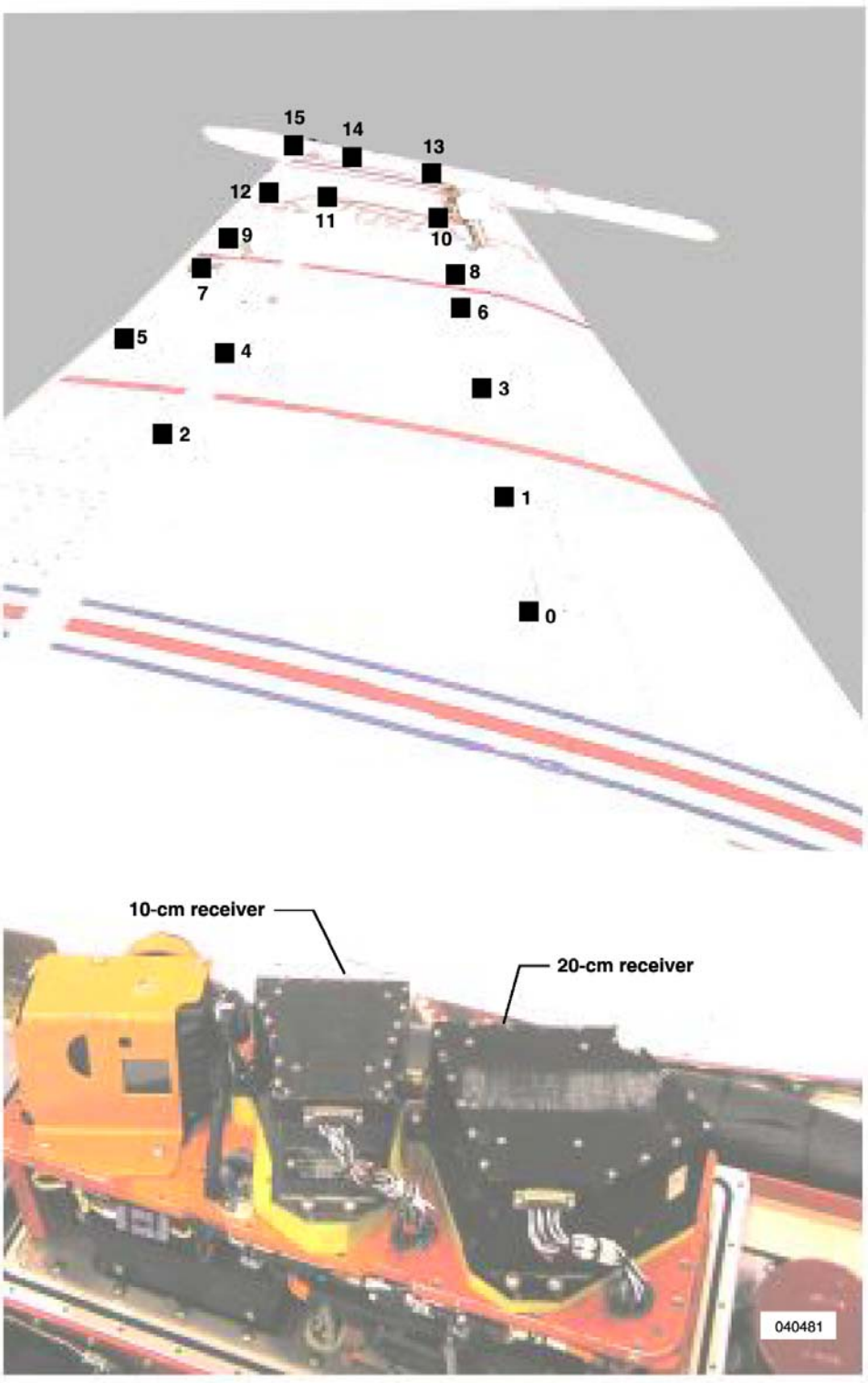

(b) Outboard view with pod off and aircraft ground stationed.

Figure 2. Concluded.

Instrumentation Accuracy

With any measurement device, measurement precision is an important consideration. Figure 3 shows worst-case single scan deflection and twist resolution magnitudes for each twist station. These plots are derived from target-to-receiver distance, target-to-target chord length, and receiver focal length. Similar to the X-29 FDMS setup, the vertical field of view for each target was resolved into 1024 data counts. The broadest possible error band of a single measurement is ±2 counts. Calibration error may be reduced to approximately ±0.25 counts over the calibration range, making this error negligible on total measurement system accuracy. Trending the deflection or twist data throughout an interval of time allows the effective measurement error to approach zero. This minimally effective measurement error is caused by the calibration error yielding results much better than this worst-case plot.

As a result of using two receivers with different focal lengths, the corresponding pairing of targets to the receivers made the deflection resolution at span station 193.8 (fig. 2(a)) better than any other span. Figure 3 shows the twist resolution is also much better at span station 193.8, whereas twist and deflection resolutions at span 165.8 are the worst. It is also important to mention that spans 154.5 and 222.1 possess nearly the same twist resolution.

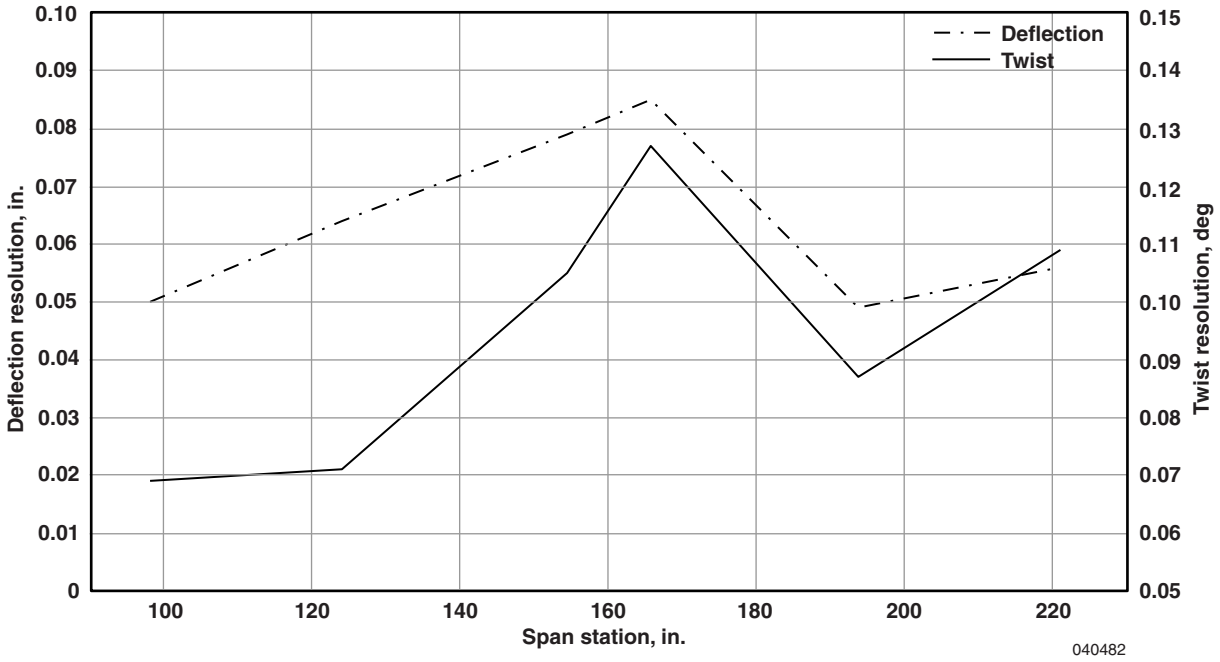

Figure 3. AAW FDMS deflection and twist resolution.

Project Phase-1 Objectives

From November 2002 through June 2003, the AAW program flew 51 phase-1 flights to accomplish the following objectives:

- Verify the ability of the baseline control law to fly the aircraft.
- Ensure all aircraft systems and instrumentation systems are functioning correctly.
- Characterize the F/A-18 aircraft test bed, its wings, and its control surfaces to quantify the effects of the wing system flexibility as a function of Mach and dynamic pressure.
- Understand the individual effectiveness of the control surfaces.
- Understand the wing box aeroelasticity as a control power-producing device across the flight test envelope.
- Understand how and where control reversal occurs for the AAW F/A-18 aircraft.

Table 1 shows the flight envelope to reach these objectives, which consisted of 18 primary flight conditions. Approximately 430 maneuvers were flown from the primary flight conditions and approximately 70 maneuvers were flown at intermediate conditions, for example Mach 0.93 at an altitude of 10,000 ft.

Table 1. AAW phase-1 flight envelope.

	Mach					
Altitude, ft	0.85	0.90	0.95	1.10	1.20	1.30
25,000				X	X	X
20,000				X	X	X
15,000	X	X	X	X	X	
10,000	X	X	X	X		
5,000	X	X	X			

Determination of control-surface effectiveness using parameter identification techniques[8] was performed with the use of the onboard excitation system (OBES)[9] to produce doublet maneuvers. Independent of the pilot, a predetermined schedule allowed the OBES to vary each control-surface position. Collective (symmetric control-surface excitation) and differential (asymmetric control-surface excitation) doublet maneuvers were performed for each control surface in a buildup approach from low- to high-magnitude deflections. Figure 4 illustrates a small differential doublet control-surface deflection time history. Table 2 shows deflections for small, medium, and large collective OBES maneuvers and table 3 shows similar data for differential OBES maneuvers.

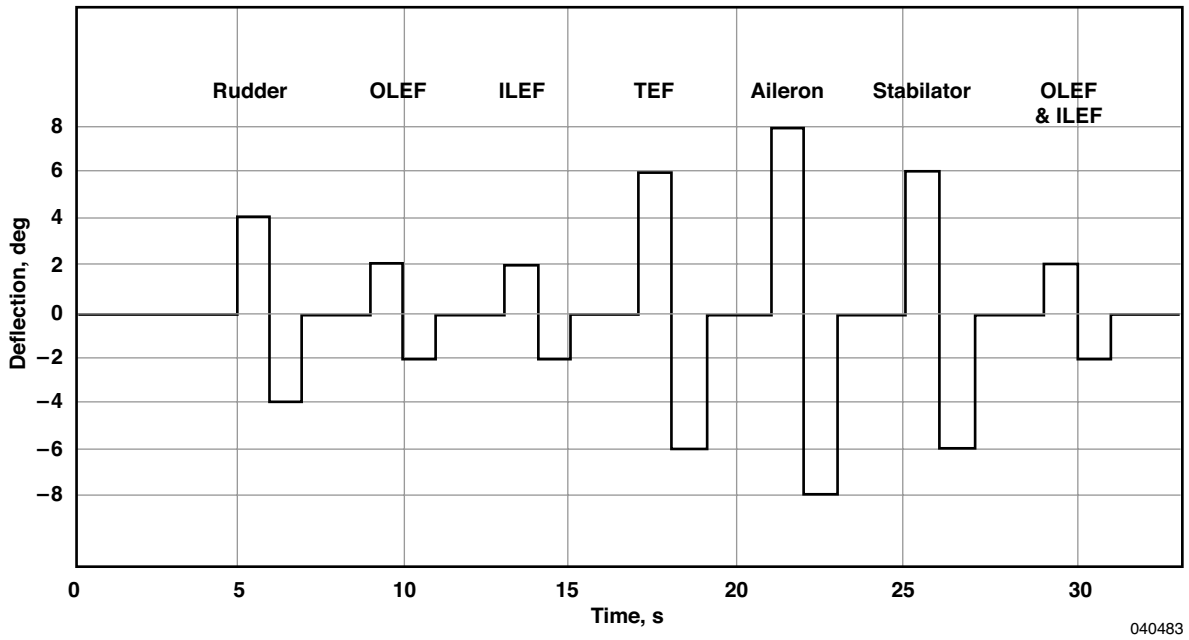

Figure 4. Small differential doublet control-surface deflection time history.

Table 2. Collective OBES doublet maneuvers for parameter identification.*

OBES Reference	OLEF	ILEF	TEF	OLEF and ILEF	Aileron	Stabilator
Large	3	3	5	3	6	0.8
Medium	2	2	4	2	5	0.8
Small	1	1	3	1	4	0.8

* Numerical values are represented in degrees.

Table 3. Differential OBES doublet maneuvers for parameter identification.*

OBES Reference	Rudder	OLEF	ILEF	TEF	Aileron	Stabilator	OLEF and ILEF
Large	4	6	6	10	12	6	6
Medium	4	4	4	8	10	6	4
Small	4	2	2	6	8	6	2

* Numerical values are represented in degrees.

To evaluate the linearity assumed in the twist model derived from standard OBES maneuvers, which produce low-twist levels only, additional maneuvers were required. Full stick rolls, wind up turns, rolling pull-outs, bank-to-bank rolls, and push-over pull-ups were also flown at each flight condition to improve twist model accuracy at high-twist levels. Approximately 370 maneuvers were used in the construction of the twist model.

Data Processing

AAW phase-1 flight data underwent many data processing steps before the data could be used to create the twist model. The following technique was initially used to develop a loads model for the AAW phase-2 control laws (CLAWS) and was applicable to twist model development.

1. Find dropouts.
2. Time synchronize data.
3. Remove data spikes.
4. Filter noise.
5. Remove stale data.
6. Calculate new parameters.

In order to find dropouts, each time signal was checked for missing time points. If missing points were found, they were filled with interpolated points and all signals at that sample rate were filled with interpolation as well. This step was used to remove data dropout problems from further data conditioning steps, such as spike removal and filtering. All filled points were marked and removed after filtering. The AAW aircraft data stream was provided with time tag parameters to help correlate measured signals in time. These time tags were used to correct flight data before use in twist model development. Signals that were sampled at 25 Hz (aircraft surfaces) used a time tag associated with those measurements on the 1553 bus. All other parameters were corrected with an embedded time signal. Since the 25-Hz data were reported at 20 Hz using a buffer, the time delay for these signals ranged greatly. Variation in time synchronization usually ranged from 30 through 70 ms. Data spikes were identified with a derivative method and manually removed with visual inspection. The technique allowed the user to identify spikes and replaced them with linear interpolation. Filtering was accomplished using forward and backward low-pass Butterworth filters. Filter bandwidths were chosen to remove noise from the signal without distorting the signal. The surface positions were not filtered because these signals have low noise and because the filter sometimes added dynamics to the signal when attempting to filter a sharp OBES doublet. Additional time points from any oversampled time signal were tagged as invalid. These tagged points, as well as dropouts found in step 1 and spikes found in step 3, were removed from the data set in step 5. This removal was possible because the twist model is time invariant. Synthesized parameters were calculated from flight measurements to improve model accuracy. These parameters usually included the product of two parameters. Although 70 of these new parameters were created, the final twist model only uses a select few.

Twist Calculation

Figure 5 illustrates angle of twist, θ, at the wingtip from the vertical displacement difference, Δ, of TGT13 (target 13) and TGT15 (target 15). The fixed distance (chordwise spacing) between the two target locations is represented by δ. Actual twist may be calculated as $\theta = \sin^{-1}(\Delta/\delta)$. Though the FDMS arrangement allowed for twist calculation at six stations along the left wingspan, the outermost four stations were chosen for model development because of their high-twist output. Figure 6 shows these stations, referred to as FTWIST3 through FTWIST6.

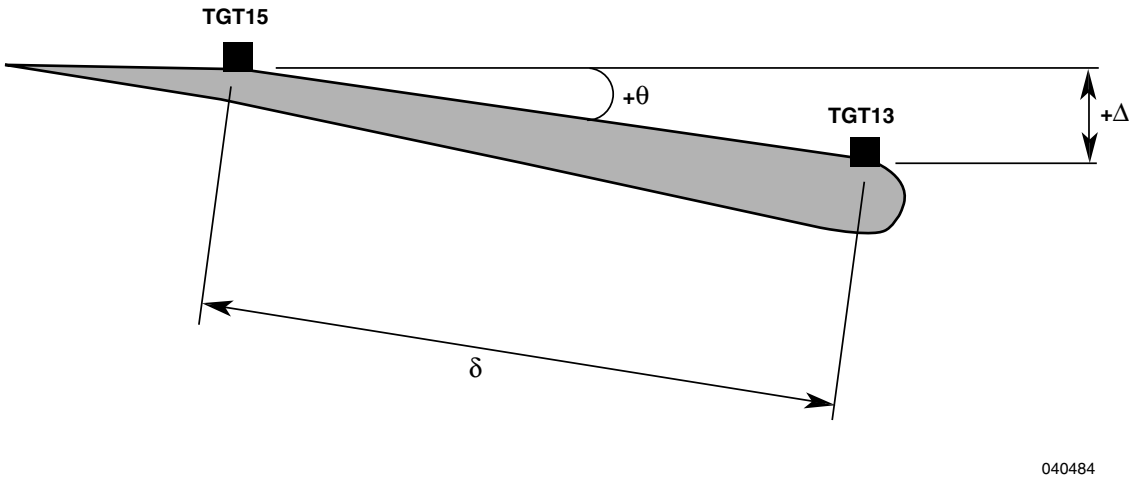

Figure 5. Wingtip twist variables.

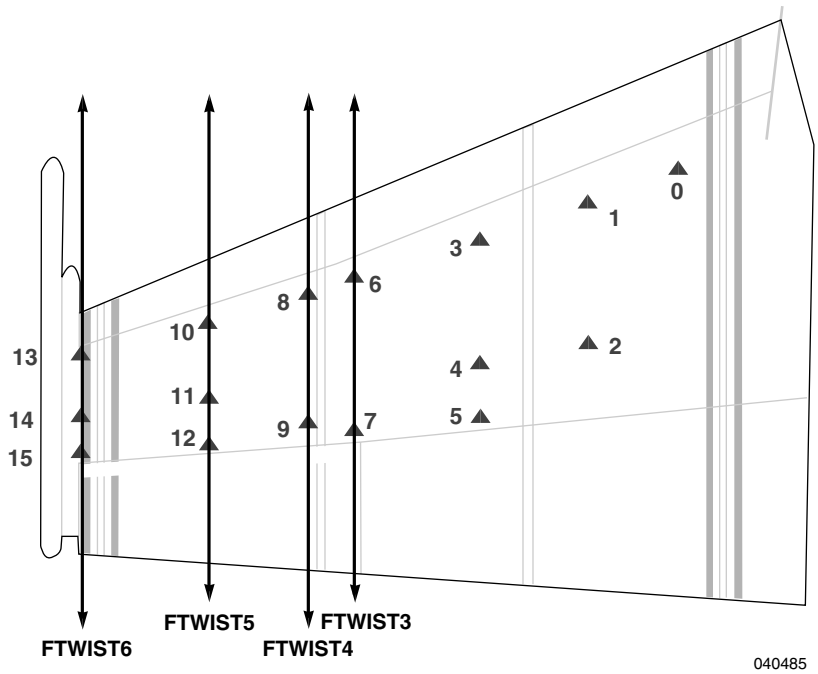

Figure 6. Modeled twist stations.

MODEL DEVELOPMENT

Model creation began by using an inhouse linear regression tool called EQuation DErivation (EQDE).[10] Predictions were developed at each of the 4 twist stations at all 18 primary flight conditions using the majority of maneuvers. A specified number of maneuvers at each flight condition were not used in model formation, but as an independent check of the model performance. After model completion, a database was created to document the twist equations and aid implementation into the AAW simulator. Figure 7 shows the original model flowchart for one twist station at one flight condition.

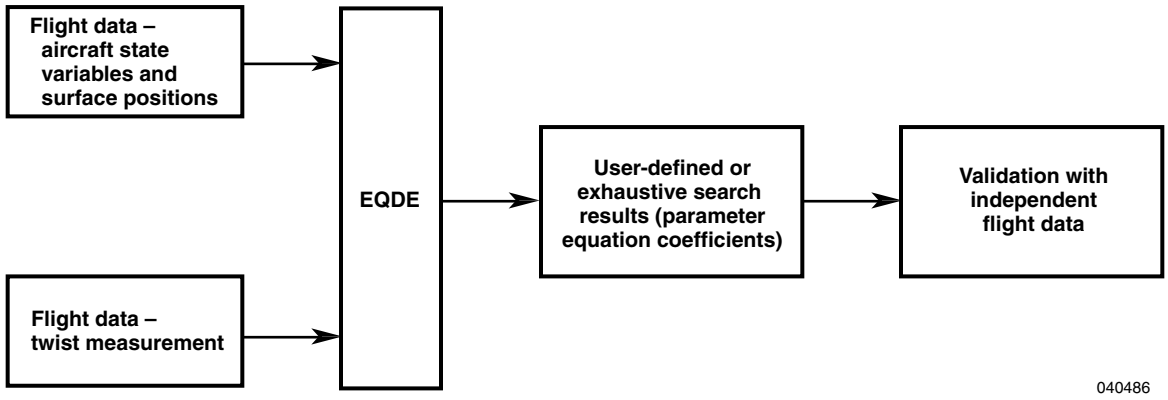

Figure 7. Original model flowchart.

Traditionally, EQDE has been used to facilitate the process of deriving loads equations from large quantities of strain gage data collected from loads calibration tests. In this case, EQDE was used to assist in the development of twist equations using large quantities of flight data from AAW phase-1 flights. The first of two primary EQDE functions was the calculation of twist influence coefficients and other statistical information for each maneuver. The influence coefficient was a measure of the correlation between parameter signal and twist undergone by the structure. Generally, parameters having larger influence coefficients produced better results. Secondly, EQDE derived equation coefficients from a given set of independent variables (aircraft state variables and surface positions, hereinafter referred to as simply ‘parameter inputs’) and a dependent variable (twist). The equation coefficients were then used to calculate twist for the model,

$$\text{Twist} = I + \sum_{i=1}^{n} P_i C_i \tag{1}$$

where n is the number of parameter inputs, C_i is the equation coefficient for the i^{th} parameter input, I is the intercept, and P_i is the i^{th} model parameter input. Equation (1) calculates a single twist at a single point in time, making the twist model time invariant.

Two approaches to run EQDE were used to attain the influence and equation coefficients. The user either explicitly specified which parameter inputs to use in the equation or the user allowed EQDE to perform an exhaustive search. The exhaustive search analyzed all possible parameter input combinations to yield an equation with a constant twist relationship relative to a specified set of parameter inputs. Both approaches were used in analysis to determine the lowest error and most reliable prediction.

The EQDE output evaluation consisted of error analysis of validation maneuvers and evaluation of measured-to-predicted time history plots. Approximately 15 percent of the maneuvers from any given flight condition were not used to create the model, but were reserved for use as an impartial check. Often , a high-twist maneuver (roll at 100-percent lateral control stick input) was used to train the model and a lower twist maneuver (roll at 50-percent stick input) was used to validate.

After deriving equations for the four twist stations at each of the flight conditions, a database was created to document the model intercept and coefficient terms. Aside from an ordered documentation of the model results, the database was used for preflight twist analysis within the simulator. Each twist station was described by one line of the twist model database. The twist model database indicated each flight condition as well as parameter input names, intercept, and model coefficients for each twist station. Table 4 is a section of the twist model database. The database lines define twist models for twist stations 3 through 6 (FTWIST3 through FTWIST6) at the flight condition of Mach 0.85 at an altitude of 15,000 ft (abbreviated as 085m15k). The intercept for the twist station 3 twist equation is 42.84. The same row gives all other model coefficients for the twist station 3 equation. Parameter inputs not used in the final equation for twist station 3 (Mach and Altitude) are set to zero.

Table 4. Sample of twist model database.

085m15k							
	Intercept	Mach	Altitude	Velocity	LAilLVDT	Alpha	Beta
FTWIST3	4.2840E+001	0.0000E+000	0.0000E+000	0.0000E+000	0.0000E+000	8.9110E+001	0.0000E+000 …
FTWIST4	–2.2301E+001	0.0000E+000	0.0000E+000	0.0000E+000	0.0000E+000	0.0000E+000	–4.9660E+000 …
FTWIST5	–6.2801E+001	0.0000E+000	0.0000E+000	0.0000E+000	0.0000E+000	0.0000E+000	4.9660E+000 …
FTWIST6	8.9110E+001	0.0000E+000	0.0000E+000	0.0000E+000	0.0000E+000	0.0000E+000	0.0000E+000 …
.	.	.	.	.	.	.	.
.	.	.	.	.	.	.	.
.	.	.	.	.	.	.	.

DYNAMIC PRESSURE ASSUMPTION AND NEURAL NET MODEL DEVELOPMENT

Independent of the original model described previously, this section describes two alternative techniques for wing-twist prediction. The dynamic pressure assumption (DPA) method predicts twist based on the aircraft dynamic pressure state instead of specific flight condition used with the original model. The second method employs neural nets to further reduce the final original model error.

Dynamic Pressure Assumption

One of the drawbacks to the original model was reduced model accuracy when the flight condition was different than the design condition. In order for the model to predict (for example, Mach 1.22 at an altitude of 20,000 ft), either the bounds of models Mach 1.20 at an altitude of 20,000 ft and Mach 1.30 at an altitude of 20,000 ft must be opened or there would have to be interpolation between the two models. The former was the preferred technique and implemented within the manned flight simulator. Interpolation was not the preferred technique because of complexity and increased processing time.

Ability to monitor real-time twist, free of flight condition constraints, could be extremely beneficial. One all-encompassing equation based on measured aircraft dynamic pressure may achieve this monitoring ability. Besides the ability to predict twist at any point, calculation using this single equation would decrease control room processing time by an order of magnitude. In order to determine this relationship, a limited DPA study was performed with supersonic data at six flight conditions with one twist station. Figure 8 shows a simple flowchart of this process.

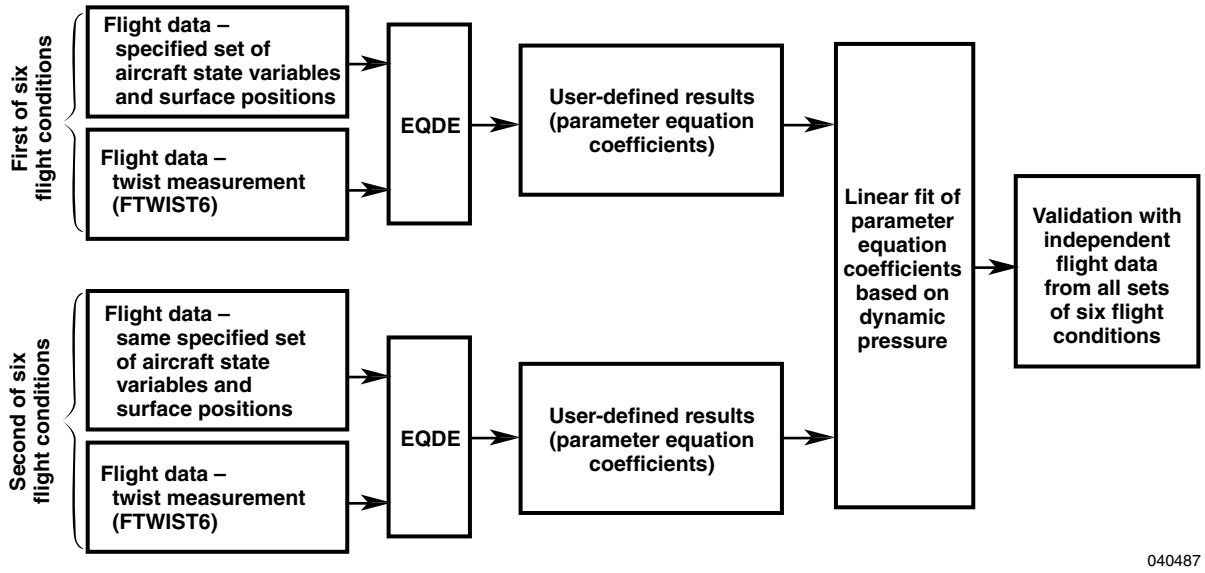

Figure 8. DPA flowchart.

Wingtip twist (FTWIST6) was modeled with EQDE at the supersonic flight conditions in table 5 with constant parameter inputs. This supersonic, low dynamic pressure region was chosen because of the low error produced at the wingtip and high quality of measured data. Parameter input equation coefficients were plotted compared with their corresponding dynamic pressure value to determine a linear relationship between the two. Figure 9 plots examples of a few parameter inputs compared with dynamic pressure. This plot shows a linear fit of the parameter inputs with dynamic pressure in grey and relative flight condition dynamic pressure on the *x*-axis.

Table 5. DPA envelope.

	Mach					
Altitude, ft	0.85	0.90	0.95	1.10	1.20	1.30
25,000				X	X	X
20,000				X	X	X
15,000						
10,000						
5,000						

Using this assumption, all of the maneuvers in the flight envelope (table 5) have an influence on the model, not just maneuvers from each flight condition as with the original model. The benefit is a data set from a broader pool of maneuvers, which may compensate for specific flight condition inadequacies. For example, all FDMS data from the 4-*g* rolling pull-out maneuvers at Mach 1.30 at an altitude of 25,000 ft were unusable because of poor flight data quality. This unsuitability appears to have little effect on the left outboard leading-edge flap rotary variable displacement transducer (LOLEFRVDT) position coefficient; however, the left aileron linear variable displacement transducer (LAilLVDT) position coefficient is far from the linear assumption. This method assumes, with ideal flight data at Mach 1.30 at an altitude of 25,000 ft, that the equation coefficient would be much closer to the linear fit. Equation (2) is used for this assumption.

$$\text{Twist}_{\text{DPA}} = C_t \bar{q} + I_t + \sum_{i=1}^{n} P_i (C_i \bar{q} + I_i) \tag{2}$$

C_t is the equation intercept coefficient, I_t is the intercept coefficient, n is the number of parameter inputs, C_i and I_i are the equation coefficient and intercept for the i^{th} parameter input, respectively, and P_i is the i^{th} model parameter input. Equation (2) is similar to the original model equation; however, it is valid over the specified flight envelope as long as the dynamic pressure, $\bar{q}$, is known. The use of *C*s and *I*s represent the slopes and intercepts of the linear fit of the parameter inputs plotted in figure 9.

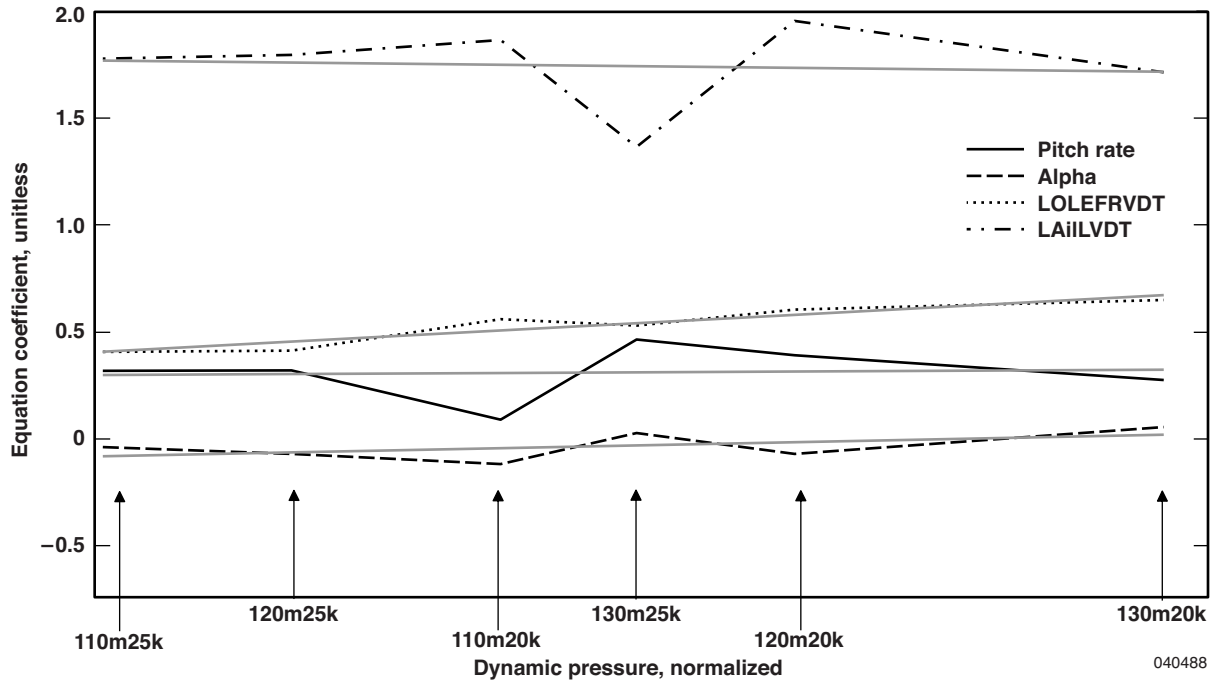

Figure 9. Equation coefficient compared with scaled dynamic pressure.

Using the previous example, a specific equation was determined at Mach 1.20 at an altitude of 20,000 ft, but valid from Mach 1.16 at an altitude of 20,000 ft through Mach 1.22 at an altitude of 20,000 ft. Although this technique allows twist prediction at virtually any Mach and altitude, flight at the boundary edge typically produced high error. Also, figure 10 shows that crossover from one boundary to the next creates a step in the data. The top plot displays a simulated slow acceleration followed by a brief deceleration with a Mach output range from 1.10 through 1.23 at an altitude of 20,000 ft. Original model boundaries as stated previously are indicated with a dash-dot line. As the Mach level passes these boundaries, the black trace on the bottom plot shows a step occurs with the original model. Independent of flight condition, the dashed trace shows DPA results indicate a smooth transition.

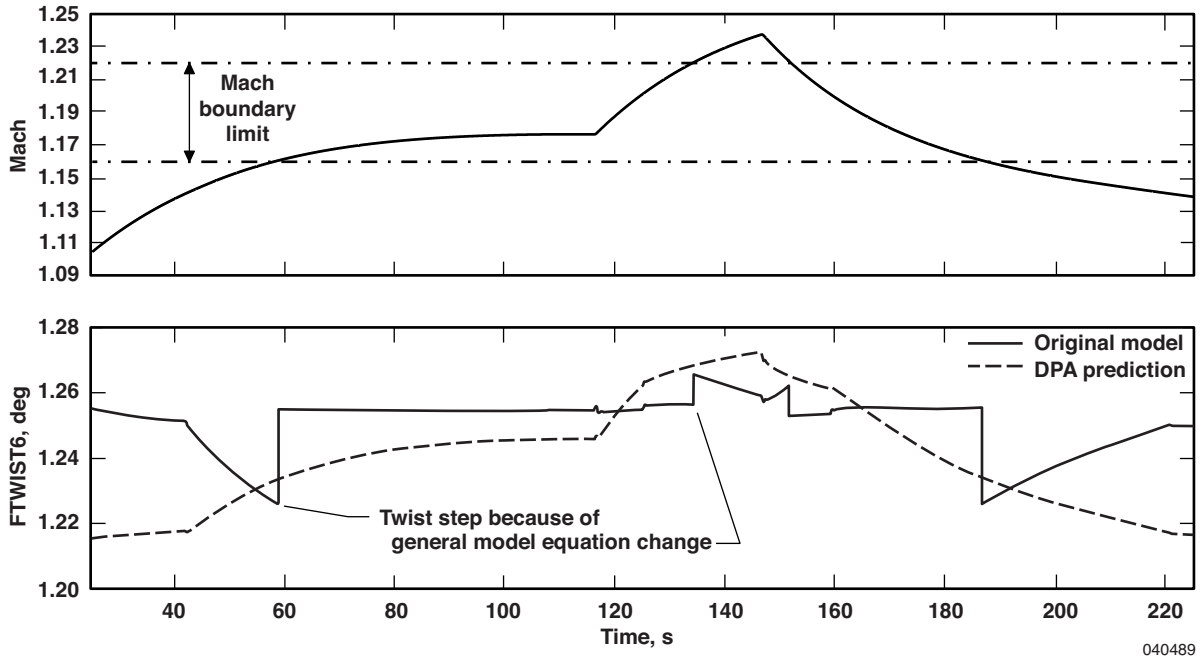

Figure 10. Original model wingtip twist step, 20,000 ft.

Neural Net Application

As a result of their ability to model nonlinear behavior, neural networks were selected for further twist model development. A neural network is a collection of fixed functions with variable gains and biases. This study used single-hidden-layer feedforward neural networks, which consisted of an input layer, hidden layer, and output layer. Figure 11 illustrates an overall process flowchart incorporating neural nets, and figure 12 is a partial depiction of a typical single-hidden-layer neural network.

Eight-node neural networks were chosen for this study from the results of parametric studies using similar data.[11] The original twist models were used to initialize the neural network models with the same parameter input set. This initialization was accomplished by neural network training with output from the original model with random input. This method of using original models to initialize the neural network models improved overall model accuracy and reduced the number of neural network training iterations required for convergence.

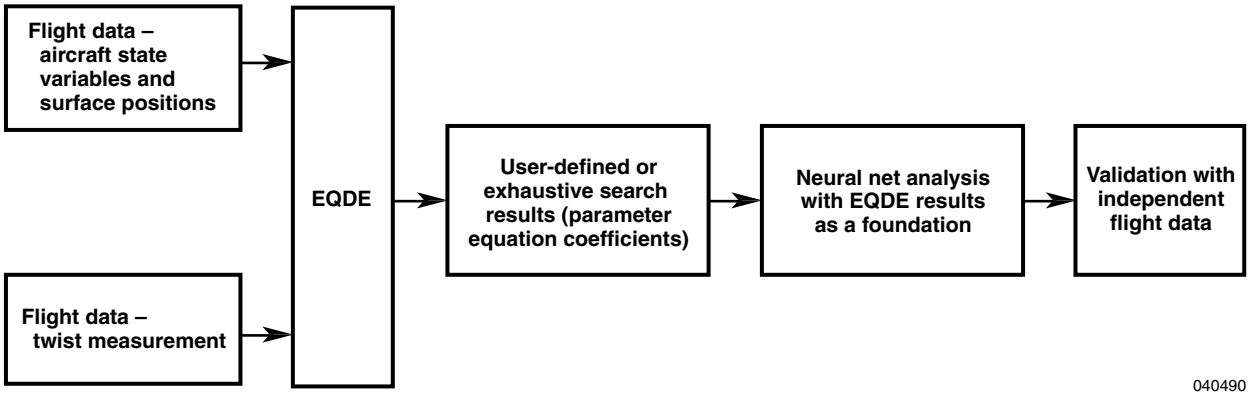

Figure 11. Neural net flowchart.

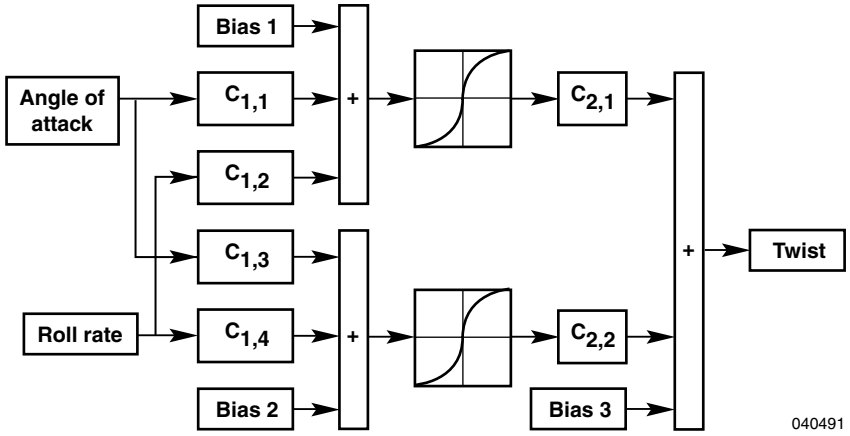

Figure 12. Typical single-hidden-layer neural network with two parameter inputs.

This study used back propagation with Levenberg-Marquardt optimization.[12] To improve generalization, this study also used neural network gain weighting with Bayesian regulation.[13] Despite these measures to improve generalization, early stopping was also employed because overtraining was still possible with the limited data set in nonlinear regions. Early stopping used separate validation data to halt neural network training when additional training cycles no longer improve the model accuracy. These steps, along with a small network size, ensured that the neural network would not overfit the training data.

RESULTS

This section compares measured twists at the four stations with predicted twists from the original model, DPA, and neural network. Although 18 primary flight conditions exist, results from specific maneuvers that represent a majority of twist behavior are presented.

As stated previously, individual control-surface effectiveness was determined with the use of doublet maneuvers at each flight condition. Figure 13 shows a typical small differential doublet maneuver and resultant measured wing twist at Mach 1.10 at an altitude of 20,000 ft. The top graph shows the individual control-surface doublet deflection in degrees and the bottom graph illustrates the absolute angle of twist in degrees of the wing at the four measured stations. Approximately 30 s of useful data from this maneuver is plotted. Twist measurement station values referenced to ground rest are shown as 0.4, 0.5, 0.8, and 1.1 for FTWIST3, FTWIST4, FTWIST5, and FTWIST6, respectively, at this flight condition. Twist magnitude increases spanwise from a maximum of about 0.9 at FTWIST3 through 1.9 at FTWIST6. From this maneuver, the rudder doublet has virtually no direct linear relationship on wing twist, whereas the combined inboard and outboard doublet has a significant effect on twist for the minor control-surface deflection (2 deg). At each of the four twist stations, the aileron doublet produced the highest overall twist and in general appears to have the most significant influence on twist.

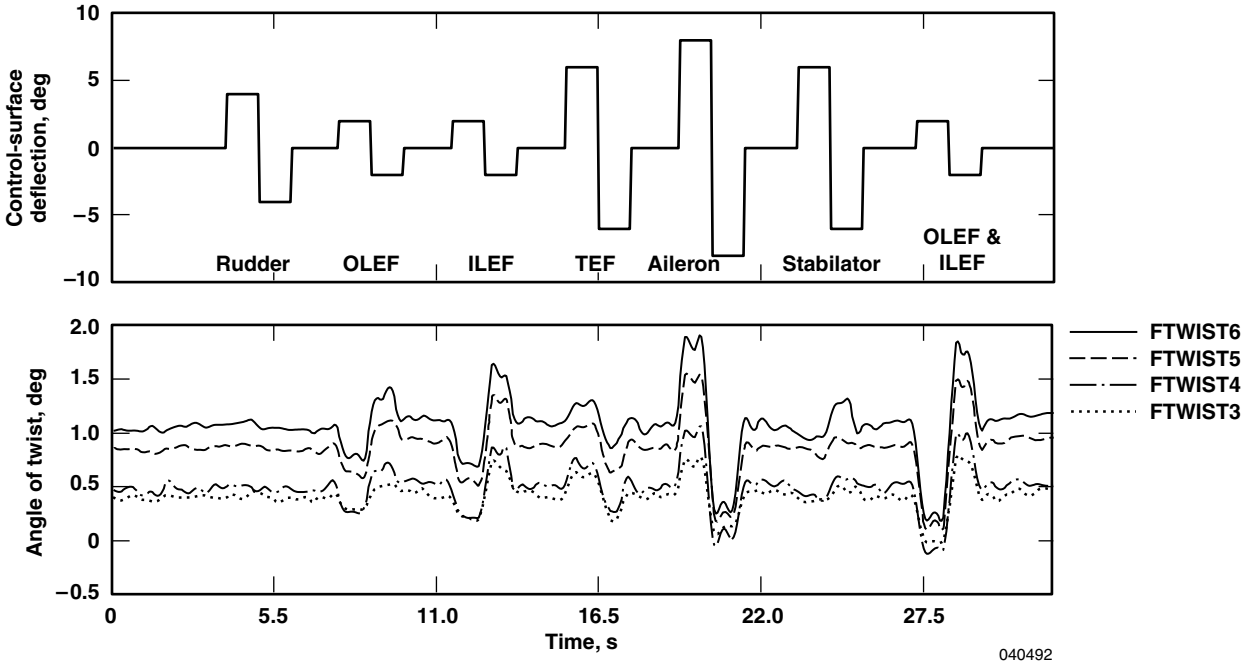

Figure 13. OBES doublet control-surface deflection and measured twist time history.

Establishment of the signal to be modeled and influence of each control surface was not enough to produce reliable twist predictions. Intuition combined with EQDE exhaustive search capability allowed determination of the optimal set of control-surface positions and aircraft state variables. Typically, the four main wing control surfaces (ILEF, OLEF, trailing-edge flap (TEF), and aileron) were used in concert with the aircraft angle of attack, roll rate, and normal acceleration inputs to minimize error between original model predictions and measured twist.

Two metrics were used to quantify the original model results. The first metric was standard root mean square (RMS) error (eq. (3)),

$$\mathrm{RMS} = \left[\frac{\sum_{l=1}^{k} (M_l - R_l)^2}{k} \right]^{\frac{1}{2}} \tag{3}$$

where k is the number of samples, M_l is the measured twist of sample number l, and R_l is the predicted twist of sample l. RMS error is one of the most commonly used statistical measures of success. The lower the RMS error, the more accurate the predicted trace follows that of the measured signal. The calculation allows each specific twist station to be individually compared over all flight conditions.

Another metric used to evaluate results is defined as the RMS error at a particular flight condition station divided by the twist angle range, $\mathrm{T_{Range}}$, of the same station for that particular flight condition (eq. (4)).

$$\mathrm{RMS_{Norm}} = \frac{\mathrm{RMS}}{\mathrm{T_{Range}}} \times 100 \tag{4}$$

This normalized percentage allows a direct comparison not only within flight conditions, but between twist stations as well. Once again, a lower $\mathrm{RMS_{Norm}}$ error indicates a strong correlation between measured and predicted signals.

Figure 14 shows original model twist prediction results of the aforementioned small differential doublet. The figure illustrates measured absolute angle of twist and the corresponding twist prediction at the four twist stations. Model predictions in each plot were created from different optimal sets of parameter inputs based on EQDE results. Approximately 12 maneuvers at Mach 1.10 at an altitude of 20,000 ft were used to train the model and 3 maneuvers were used to validate the prediction.

Figure 14 also displays the two metrics discussed previously. The term *training* quoted in the marginal table of this figure refers to the metric calculated from the dozen maneuvers used to derive equation coefficients. This training error provides insight to the linearity of maneuvers used to create the model. The term *validation* quoted in the marginal table refers to the error calculated from the three maneuvers set aside as an independent check of the model. The validation error reflects how well the model predicts maneuvers from the same flight condition that were not used to create the model. Observation shows that the training error is greater than the validation error in some cases and is common because of the higher twist-producing maneuvers used for training. Table 6 presents a summary of errors from the entire flight envelope.

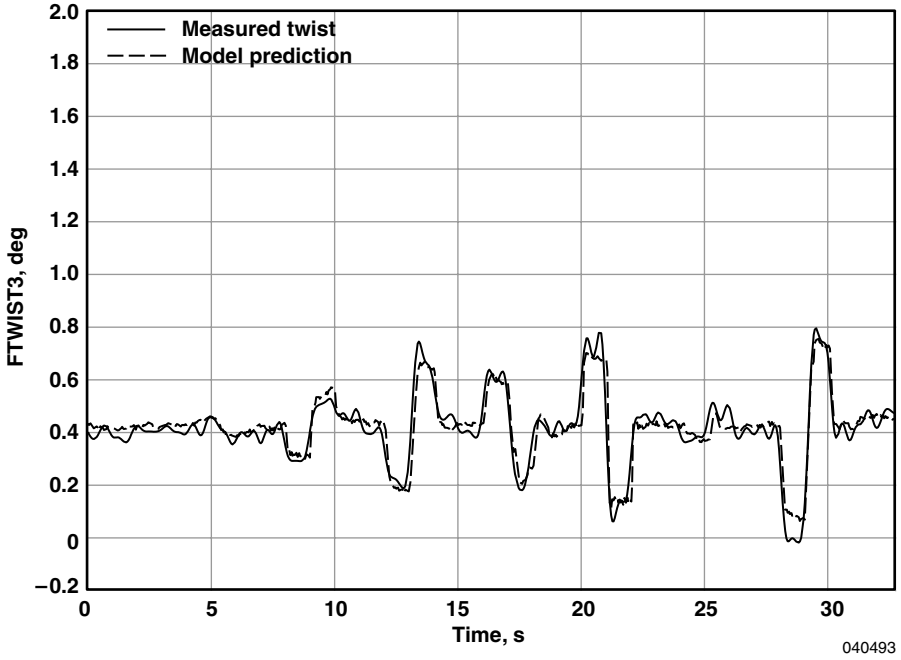

FTWIST3 Mach 1.10 at 20,000 ft

RMS error, deg	
Training	Validation
0.050	0.064
RMS_{Norm} error, percent	
Training	Validation
4.14	6.43

(a) FTWIST3 time history.

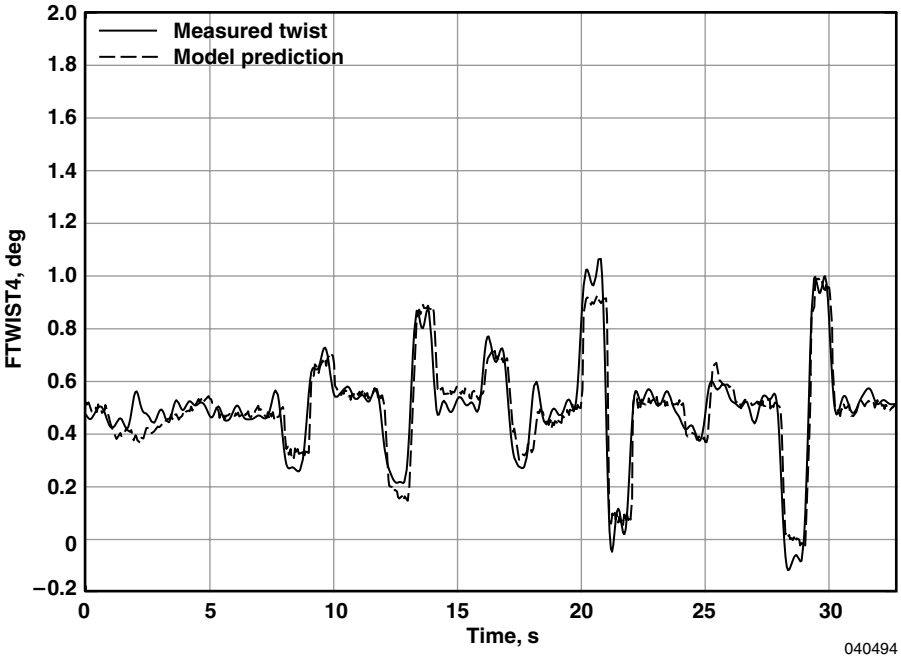

FTWIST4 Mach 1.10 at 20,000 ft

RMS error, deg	
Training	Validation
0.088	0.085
RMS_{Norm} error, percent	
Training	Validation
2.78	7.15

(b) FTWIST4 time history.

Figure 14. Mach 1.10 at an altitude of 20,000 ft total error and medium differential doublets plot.

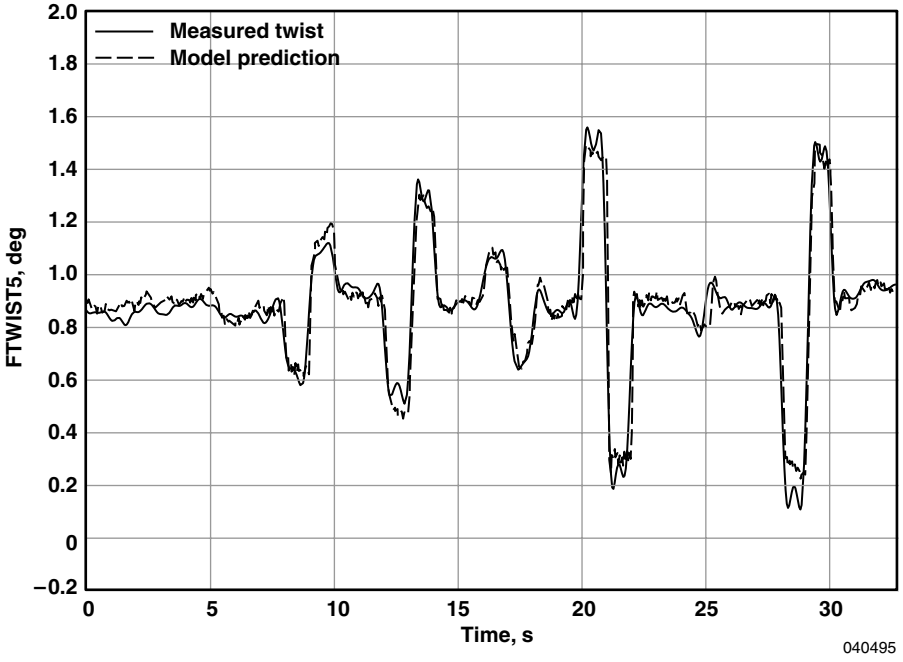

FTWIST5 Mach 1.10 at 20,000 ft

RMS error, deg	
Training	Validation
0.076	0.082
RMS_{Norm} error, percent	
Training	Validation
3.66	5.30

(c) FTWIST5 time history.

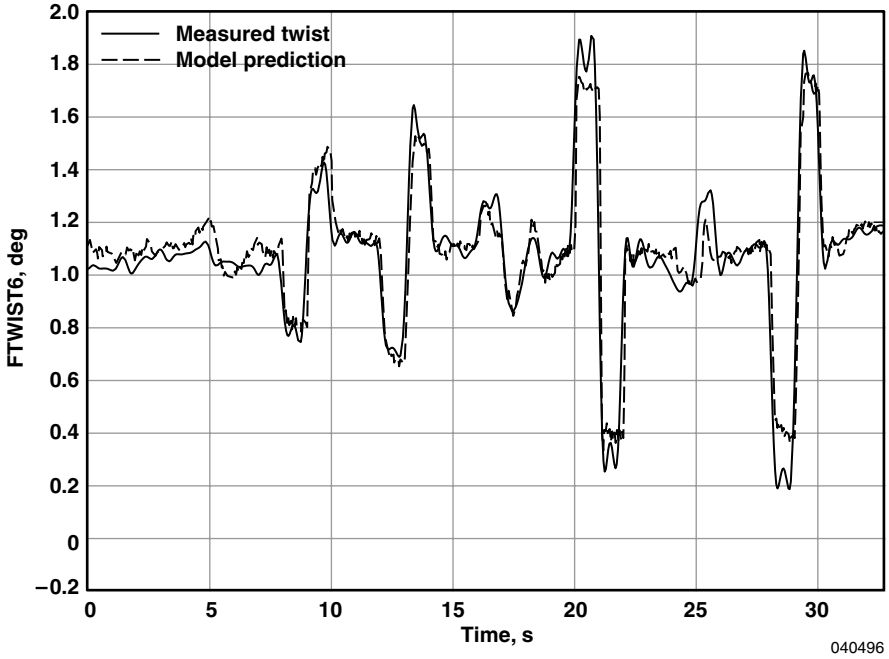

FTWIST6 Mach 1.10 at 20,000 ft

RMS error, deg	
Training	Validation
0.096	0.106
RMS_{Norm} error, percent	
Training	Validation
4.00	6.15

(d) FTWIST6 time history.

Figure 14. Concluded.

Table 6(a). Complete envelope RMS and RMS_{Norm} errors: FTWIST3.

	RMS error, deg		RMS_{Norm} error, percent	
	Training	Validation	Training	Validation
085m05k	0.111	0.081	2.77	4.01
085m10k	0.116	0.072	3.79	3.80
085m15k	0.090	0.065	2.80	4.89
090m05k	0.117	0.103	3.88	7.14
090m10k	0.095	0.102	3.84	4.96
090m15k	0.090	0.105	2.72	5.11
095m05k	0.085	0.074	5.88	6.06
095m10k	0.067	0.068	5.41	6.17
095m15k	0.078	0.064	2.75	5.67
130m25k	0.055	0.066	5.97	8.04
130m20k	0.043	0.042	4.56	8.12
120m25k	0.046	0.056	4.18	7.60
120m20k	0.042	0.056	4.90	6.57
120m15k	0.061	0.053	6.42	7.00
110m25k	0.058	0.060	4.68	6.50
110m20k	0.050	0.064	4.14	6.43
110m15k	0.058	0.076	5.02	7.32
110m10k	0.050	0.039	4.87	5.08

Table 6(b). Complete envelope RMS and RMS_{Norm} errors: FTWIST4.

	RMS error, deg		RMS_{Norm} error, percent	
	Training	Validation	Training	Validation
085m05k	0.157	0.150	3.01	4.43
085m10k	0.230	0.195	5.31	7.42
085m15k	0.184	0.143	4.87	6.64
090m05k	0.140	0.101	3.65	5.09
090m10k	0.266	0.256	5.50	9.10
090m15k	0.173	0.172	4.95	6.94
095m05k	0.094	0.090	4.87	5.57
095m10k	0.090	0.084	5.17	5.03
095m15k	0.116	0.105	4.52	7.02
130m25k	0.158	0.111	5.61	11.64
130m20k	0.057	0.052	4.71	6.16
120m25k	0.112	0.231	3.69	9.78
120m20k	0.185	0.137	7.50	11.29
120m15k	0.082	0.073	6.20	7.42
110m25k	0.122	0.107	4.19	7.74
110m20k	0.088	0.085	2.78	7.15
110m15k	0.224	0.124	7.43	8.93
110m10k	0.062	0.052	4.26	4.79

Table 6(c). Complete envelope RMS and RMS_{Norm} errors: FTWIST5.

	RMS error, deg		RMS_{Norm} error, percent	
	Training	Validation	Training	Validation
085m05k	0.208	0.170	2.97	3.54
085m10k	0.175	0.114	3.47	3.32
085m15k	0.160	0.111	2.91	4.53
090m05k	0.204	0.168	3.69	4.60
090m10k	0.207	0.153	4.50	3.90
090m15k	0.141	0.178	2.20	4.49
095m05k	0.135	0.119	5.95	4.98
095m10k	0.101	0.105	3.87	4.55
095m15k	0.127	0.116	2.45	5.59
130m25k	0.078	0.071	4.15	5.42
130m20k	0.075	0.081	4.70	6.10
120m25k	0.060	0.070	3.33	4.73
120m20k	0.080	0.078	4.88	4.96
120m15k	0.095	0.056	5.95	4.25
110m25k	0.069	0.068	3.71	4.29
110m20k	0.076	0.082	3.66	5.30
110m15k	0.095	0.103	4.37	5.55
110m10k	0.098	0.087	4.93	6.01

Table 6(d). Complete envelope RMS and RMS_{Norm} errors: FTWIST6.

	RMS error, deg		RMS_{Norm} error, percent	
	Training	Validation	Training	Validation
085m05k	0.245	0.154	3.19	2.92
085m10k	0.193	0.178	3.40	3.26
085m15k	0.208	0.148	3.28	5.31
090m05k	0.254	0.276	4.09	6.25
090m10k	0.191	0.148	3.85	3.42
090m15k	0.165	0.170	2.19	4.13
095m05k	0.159	0.155	6.26	5.63
095m10k	0.141	0.106	4.41	3.79
095m15k	0.159	0.140	2.89	6.00
130m25k	0.089	0.100	4.40	5.87
130m20k	0.091	0.082	5.51	6.02
120m25k	0.113	0.078	4.87	4.44
120m20k	0.091	0.080	4.51	4.31
120m15k	0.159	0.104	8.71	7.05
110m25k	0.125	0.070	4.86	4.26
110m20k	0.096	0.106	4.00	6.15
110m15k	0.115	0.142	4.60	7.16
110m10k	0.113	0.130	4.43	7.55

Considerably more maneuvers comprised subsonic flight conditions. This ultimately led to higher quality models than those at supersonic conditions. The optimal subsonic and supersonic results occurred at Mach 0.85 at an altitude of 5,000 ft and Mach 1.10 at an altitude of 20,000 ft, respectively, based on the average errors from all four twist stations. Higher dynamic pressure conditions produced higher errors as shown at Mach 0.95 at an altitude of 5,000 ft and Mach 1.20 at an altitude of 15,000 ft.

The most consistent station to model was FTWIST5, whereas FTWIST4 proved to have significant nonlinearities. These inaccuracies may be the result of aerodynamically induced control-surface deformation or poor twist resolution discussed previously. Control-surface aeroelasticity most likely contributes a large roll in twist model error and is a topic for another study.

As mentioned previously, maneuvers other than OBES doublets were used to develop each model. Figure 15 illustrates a typical 45-deg bank-to-bank maneuver using 23-percent lateral stick deflection. The graph shows the wingtip-measured twist original model prediction and DPA prediction. In nearly all of the six flight conditions used to create the DPA, original model results compared more closely with actual twist measurements. Table 7 shows similar RMS and RMS_{Norm} error analysis for the DPA results. Also added to the table are an interpolated (Mach 1.25 at an altitude of 20,000 ft) and an extrapolated (Mach 1.20 at an altitude of 15,000 ft) flight condition. Neither condition was used in formation of the DPA; however, the dynamic pressure of Mach 1.25 at an altitude of 20,000 ft is valid for the assumption. Figure 16 shows measured and predicted twist results of a half stick 360-deg roll from the interpolated condition. Dynamic pressure from Mach 1.20 at an altitude of 15,000 ft fell outside the valid range and proved difficult to improve with the DPA. These results suggest the original model will produce superior results at specified flight conditions and the DPA provides reasonably accurate twist predictions to be monitored between specific flight conditions.

Table 7. DPA results.

	RMS error, deg		RMS_{Norm} error, percent	
	Training	Validation	Training	Validation
130m25k	0.130	0.167	6.46	9.83
130m20k	0.101	0.082	6.10	6.19
125m20k*	0.106	0.068	5.77	4.83
120m25k	0.169	0.084	7.23	4.77
120m20k	0.095	0.080	4.71	4.30
120m15k**	0.261	0.092	14.27	6.26
110m25k	0.148	0.080	5.74	4.89
110m20k	0.110	0.106	4.56	6.56

* Interpolated flight condition.
** Extrapolated flight condition.

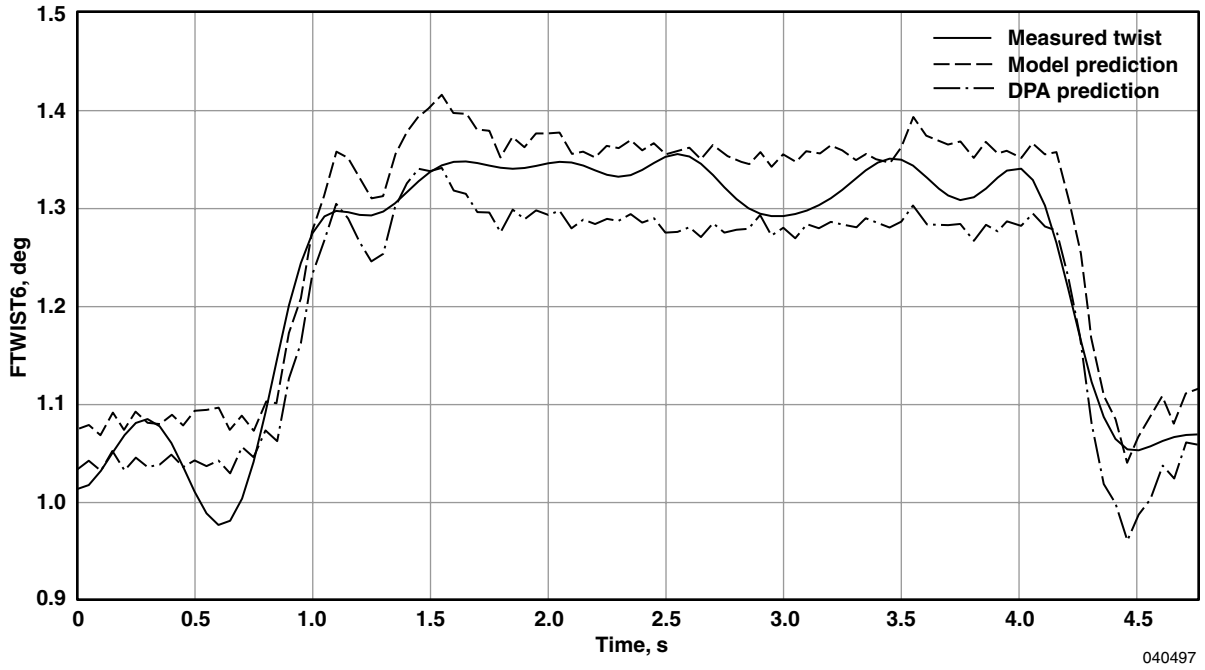

Figure 15. Mach 1.10 at an altitude of 25,000 ft, 4-deg bank-to-bank (23-percent lateral stick).

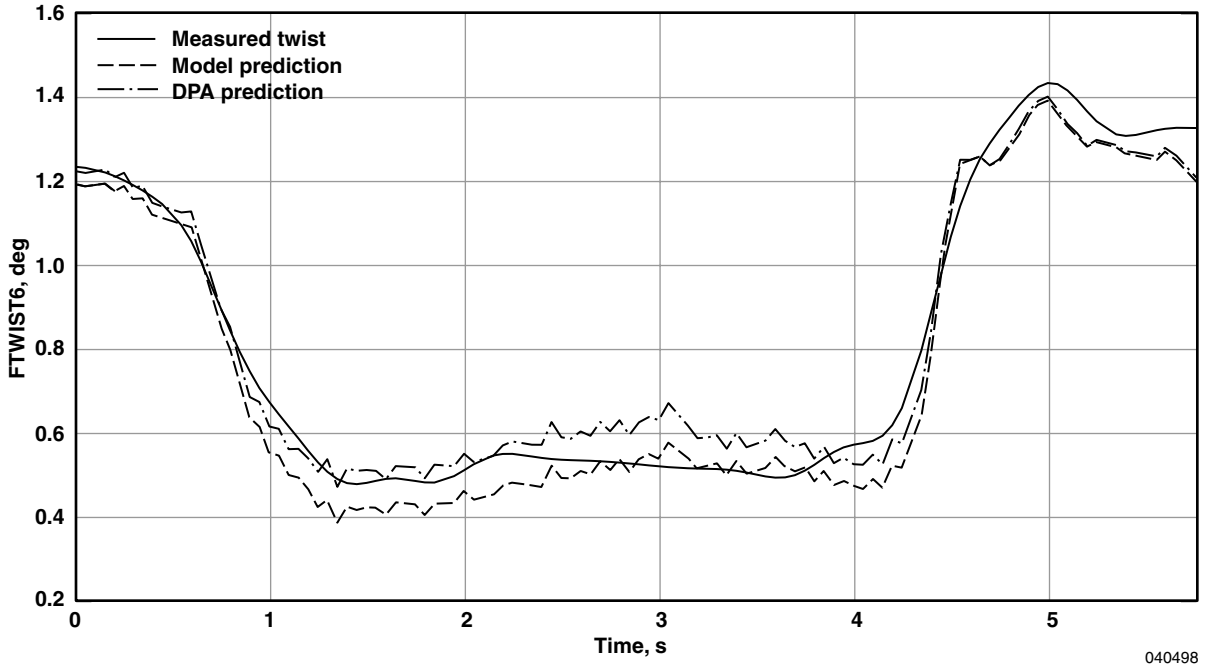

Figure 16. Mach 1.25 at an altitude of 20,000 ft, 360-deg roll (50-percent lateral stick) interpolation.

In some cases the overall highest error and unreasonable results were produced at FTWIST4. The study to determine if these nonlinearities could be lowered with the use of a neural net proved beneficial. Figure 17 and figure 18 illustrate a roll and push-over pull-up, respectively, at FTWIST4, which were dramatically corrected by using the neural net. When this technique was applied to other twist stations and flight conditions, however, the technique rarely outperformed the linear regression model.

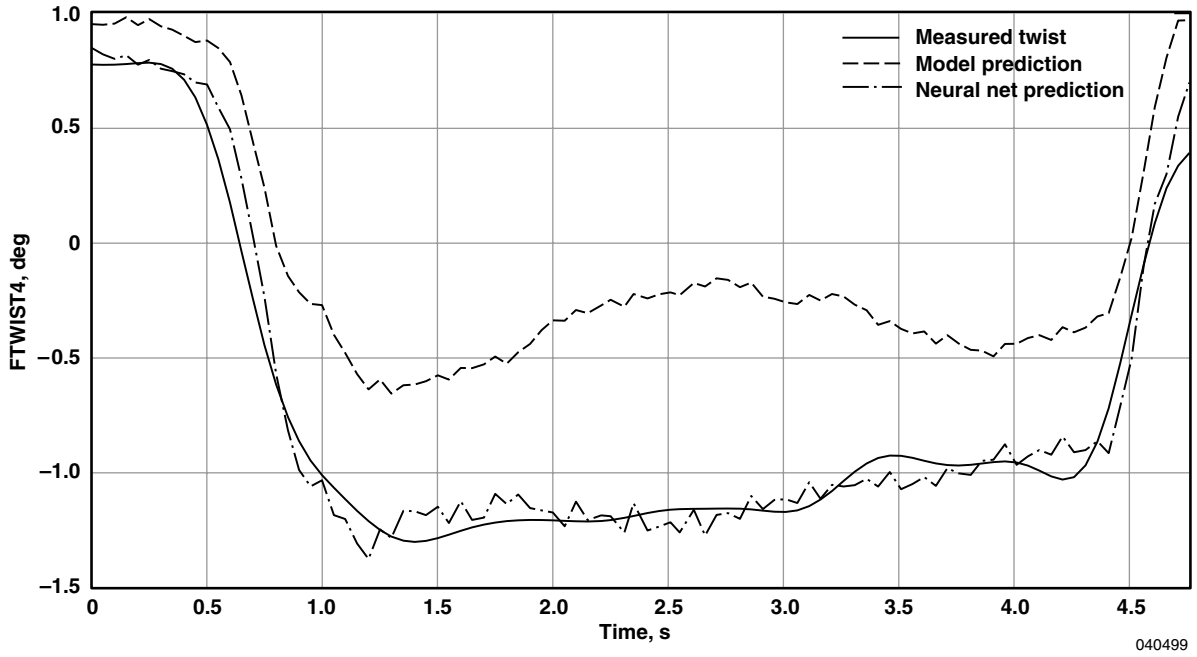

Figure 17. Mach 0.90 at an altitude of 10,000 ft, 360-deg roll (47-percent lateral stick) neural net comparison.

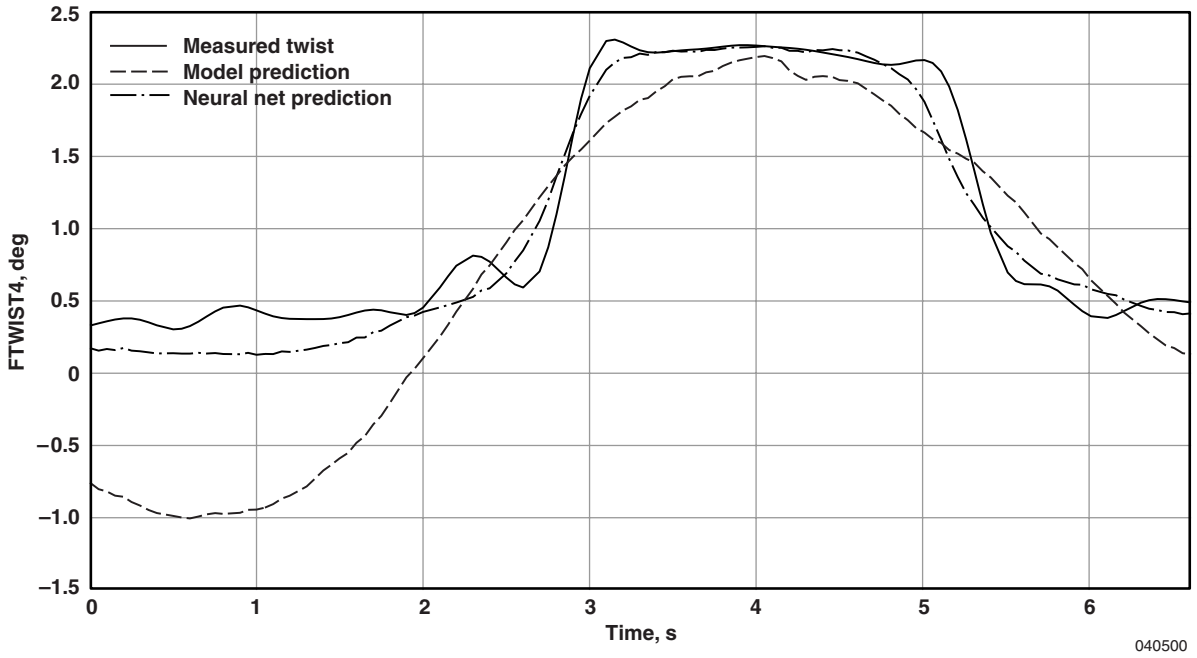

Figure 18. Mach 1.20 at an altitude of 25,000 ft, push-over pull-up (–1 through 3 *g*) neural net comparison.

CONCLUDING REMARKS

In summary, a model to predict the elastic streamwise wing twist on the active aeroelastic wing aircraft was developed to examine wing twist in the simulator, understand aircraft performance uncertainties, and assist with computational fluid dynamic and aeroelastic model development. Documentation included the instrumentation and flight data background, data acquisition, signal conditioning process, and linear regression method used to create the original model. Further model development incorporated the use of a dynamic pressure-based assumption and neural networks. Illustrative results were presented at various flight conditions and twist stations, and entire flight envelope errors were tabulated.

Original model results showed an explicit linear relationship between control-surface positions and aircraft state variables with wing twist. Typically, the most challenging flight conditions to predict were high in dynamic pressure or closer to the transonic region. Twist station 4 gave the highest overall original model prediction error, most likely as a result of the high deflection and twist resolution output of the two targets. Twist station 5 returned the lowest error overall, probably as a result of the low deflection and twist resolution. Results from the dynamic pressure assumption suggest that the original model will produce superior results at specified flight conditions and the dynamic pressure assumption provides reasonably accurate twist predictions to be monitored between specific flight conditions. A further study into the usefulness of a similar subsonic equation may prove useful. Indications of nonlinearity were present in some of the data. A neural net was used to reduce the error when nonlinearities existed and proved to accomplish this in certain situations, usually with twist station 4, but rarely outperformed the original model.

Dryden Flight Research Center
National Aeronautics and Space Administration
Edwards, California, November 4, 2004

REFERENCES

1. DeAngelis, V. Michael and Robert Fodale, "Electro-Optical Flight Deflection Measurement System," 18th Annual Symposium Society of Flight Test Engineers Proceedings, Paper 22, September 28–October 2, 1987.

2. Pendleton, Edmund W., Denis Bessette, Peter B. Field, Gerald D. Miller, and Kenneth E. Griffin, "Active Aeroelastic Wing Flight Research Program: Technical Program and Model Analytical Development," *Journal of Aircraft*, Vol. 37, No. 4, July–August 2000.

3. Lokos, William A., "Predicted and Measured In-Flight Wing Deformations of a Forward-Swept-Wing Aircraft," 21st Annual Symposium Society of Flight Test Engineers Proceedings, Paper A92-35926 14-01, August 6–10, 1990.

4. DeAngelis, V. M., "In-Flight Deflection Measurement of the HiMAT Aeroelastically Tailored Wing," AIAA/SETP/SFTE/SAE/ITEA/IEEE 1st Flight Testing Conference, Las Vegas, Nevada, AIAA-81-2450, November 11–13, 1981.

5. Powers, Sheryll Goecke, Lannie D. Webb, Edward L. Friend, and William A. Lokos, *Flight Test Results From a Supercritical Mission Adaptive Wing With Smooth Variable Camber*, NASA TM-4415, 1992.

6. Bonnema, Kenneth L. and William A. Lokos, "AFTI/F-111 Mission Adaptive Wing Flight Test Instrumentation Overview," 35th International Instrumentation Symposium, Orlando, Florida, Paper No. 89-0084, May 1–4, 1989.

7. Lokos, William A., Catherine M. Bahm, and Robert A. Heinle, *Determination of Stores Pointing Error Due to Wing Flexibility Under Flight Load*, NASA TM-4646, 1995.

8. Iliff, Kenneth W. and Kon-Sheng Charles Wang, *Flight-Determined Subsonic Lateral-Directional Stability and Control Derivatives of the Thrust-Vectoring F-18 High Angle of Attack Research Vehicle (HARV), and Comparisons to the Basic F-18 and Predicted Derivatives*, NASA/TP-1999-206573, 1999.

9. Iliff, Kenneth W. and Kon-Sheng Charles Wang, *Flight-Determined Subsonic Longitudinal Stability and Control Derivatives of the F-18 High Angle of Attack Research Vehicle (HARV) With Thrust Vectoring*, NASA/TP-97-206539, 1997.

10. Lokos, William A. and Rick Stauf, *Strain-Gage Loads Calibration Parametric Study*, NASA/TM-2004-212853, 2004.

11. Allen, Michael J. and Ryan P. Dibley, *Modeling Aircraft Wing Loads from Flight Data Using Neural Networks*, NASA/TM-2003-212032, 2003.

12. Hagan, Martin T. and Mohammad B. Menhaj, "Training Feedforward Networks with the Marquardt Algorithm," *IEEE Transactions on Neural Networks*, Vol. 5, No. 6, November 1994, pp. 989–993.

13. MacKay, David J. C., "Bayesian Interpolation," *Neural Computation*, Vol. 4, No. 3, May 1992, pp. 415–447.

REPORT DOCUMENTATION PAGE

Form Approved
OMB No. 0704-0188

1. REPORT DATE *(DD-MM-YYYY)*	2. REPORT TYPE	3. DATES COVERED *(From - To)*
10-03-2005	Technical Memorandum	

4. TITLE AND SUBTITLE

Twist Model Development and Results From the Active Aeroelastic Wing F/A-18 Aircraft

5a. CONTRACT NUMBER

5b. GRANT NUMBER

5c. PROGRAM ELEMENT NUMBER

6. AUTHOR(S)

Andrew M. Lizotte and Michael J. Allen

5d. PROJECT NUMBER

5e. TASK NUMBER

5f. WORK UNIT NUMBER

710-61-14-SE-14-00-AAW

7. PERFORMING ORGANIZATION NAME(S) AND ADDRESS(ES)

NASA Dryden Flight Research Center
P.O. Box 273
Edwards, California 93523-0273

8. PERFORMING ORGANIZATION REPORT NUMBER

H-2579

9. SPONSORING/MONITORING AGENCY NAME(S) AND ADDRESS(ES)

National Aeronautics and Space Administration
Washington, DC 20546-0001

10. SPONSORING/MONITOR'S ACRONYM(S)

NASA

11. SPONSORING/MONITORING REPORT NUMBER

NASA/TM-2005-212861

12. DISTRIBUTION/AVAILABILITY STATEMENT

Unclassified -- Unlimited
Subject Category 05 Availability: NASA CASI (301) 621-0390

13. SUPPLEMENTARY NOTES

An electronic version can be found at the NASA Dryden Flight Research Center Web site, under Technical Reports.

14. ABSTRACT

Understanding the wing twist of the active aeroelastic wing F/A-18 aircraft is a fundamental research objective for the program and offers numerous benefits. In order to clearly understand the wing flexibility characteristics, a model was created to predict real-time wing twist. A reliable twist model allows the prediction of twist for flight simulation, provides insight into aircraft performance uncertainties, and assists with computational fluid dynamic and aeroelastic issues. The left wing of the aircraft was heavily instrumented during the first phase of the active aeroelastic wing program allowing deflection data collection. Traditional data processing steps were taken to reduce flight data, and twist predictions were made using linear regression techniques. The model predictions determined a consistent linear relationship between the measured twist and aircraft parameters, such as surface positions and aircraft state variables. Error in the original model was reduced in some cases by using a dynamic pressure-based assumption and by using neural networks. These techniques produced excellent predictions for flight between the standard test points and accounted for nonlinearities in the data. This report discusses data processing techniques and twist prediction validation, and provides illustrative and quantitative results.

15. SUBJECT TERMS

Active aeroelastic wing, Aeroelasticity, Flight deflection measurement system, Reduced wing twist, Twist model development

16. SECURITY CLASSIFICATION OF:			17. LIMITATION OF ABSTRACT	18. NUMBER OF PAGES	19a. NAME OF RESPONSIBLE PERSON
a. REPORT	b. ABSTRACT	c. THIS PAGE			STI Help Desk (email: help@sti.nasa.gov)
					19b. TELEPHONE NUMBER *(Include area code)*
U	U	U	UU	34	(301) 621-0390